Residual Oil Saturation Dependence on Initial Water Saturation in Clean Water-Wet Sandstone

R. D. Hazlett[†], M. M Honarpour, J. R. Bulau, & R. N. Vaidya
Mobil E&P Technical Center

ABSTRACT

An integrated study involving network modeling and flow experiments on a suite of relatively clean unconsolidated, water-wet sandstone cores indicated an S-shaped relationship between initial water saturation, S_{iw}, and residual oil to waterflooding, S_{orw}. These core materials which contained little clay and microporosity showed minor influence of initial water saturation on residual oil in the low water saturation range. At high initial water saturation, a rather dramatic drop in residual oil saturation was observed. The trends observed in the laboratory were readily predicted by network model calculations carried out on pore-level, 3-D microtomographic images of similar rock samples. A generalized correlation was constructed relating S_{orw} and S_{iw}. Network model calculations using 3-D images of selected unconsolidated cores of the same facies type were found to obey the same general scaling relationship. Our measurements and predictions are compared with the commonly employed Land-type expression relating S_{oi} and S_{or}, as well as correlations from the literature by Agarwal and by Narr and Henderson.

The observed relationship between S_{orw} and S_{iw} for the type of rocks and fluids under investigation is explained in terms of reversible and irreversible movements of the oil-water interface. At low water saturation, interfacial movements during imbibition involve primarily the relaxation of interfaces conforming to grain/pore curvature. No phase trapping takes place in this regime since pore-filling events are absent. Consequently, S_{orw} is insensitive to small changes in initial water saturation at high capillary pressure. At higher initial water saturation, water occupies pores where irreversible oil-water interfacial movements with oil trapping potential would have occurred during imbibition if those pores had been initially oil-filled. Naturally, the absence of oil within the pore structure where oil would have been trapped yields lower residual.

The observed trends are predicted to be quite different in the presence of extensive microporosity or when a wettability-altering crude oil is used. Deviations from the S-shaped trend could serve as an indicator of wettability alteration or simply be a consequence of multiple porosity types, each with phase-trapping potential.

INTRODUCTION

The amount of nonwetting phase trapping during imbibition has been shown to be a function of the initial conditions, namely, the volume fraction of oil initially present. This feature has enormous impact in the determination of recoverable reserves from a reservoir with spatially varying initial oil (or gas) saturation. All reservoirs will exhibit saturation variation due to heterogeneity in rock characteristics and the interplay of capillary and buoyancy forces.

In addition, multiphase flow functions, modeled through relative permeability curves, are typically normalized to the mobile phase fraction. This normalization requires knowledge of trapped or noncontributing saturation elements for each phase present. Thus, a need exists for reliable scaling parameters for simulation of reservoir dynamics.

Often special core analysis laboratory work with reservoir cores is restricted to investigations with only a few selected samples due to availability and cost. Preferred methodology for imbibition flow experiments is to prepare the core to represent initial or discovery conditions with reservoir fluids at the appropriate temperature and pressure. Primary drainage porous plate

experiments are reliable means to set the initial water saturation in cores to the nominal level observed in the field. More importantly, in such experiments, fluid distribution at the pore level is set according to equilibrium, capillary-controlled conditions. Occasionally, other methods are used to prepare and run fluid flow experiments. Often, the desire for reservoir conditions is relaxed, or due to ease, time, or cost, alternative procedures are invoked. Reliable means are needed to scale experiments performed at different starting conditions, possibly due to variance in procedures. Still, limitations on the number of samples which can be investigated demands the ability to take experiments, say performed at one initial water saturation, S_{iw}, and rescale those experimental results to represent other rock regions of geometrically similar rock texture or the same rock type at different positions in the reservoir with respect to the free water level.

Narr and Henderson[1] presented a model relating saturations in drainage and imbibition processes which share the same value of nonwetting phase relative permeability. A pore-scale model was used to derive this relationship which made use of two realizations of the pore size distribution interpreted from primary drainage porosimetry data. Cylindrical capillary tubes from a first section were mated with a second set of cylindrical capillary tubes, with pore throats being defined by the reduction in tube diameter at the juncture. As a model with one-dimensional, noncommunicating elements (coordination number of unity), trapping was introduced by the artificial addition of buffer space for fluid redistribution at the pore level before the characteristic pore-level "sandwich" was repeated. This model representation of pore space, coupled with a tube bundle model for relative permeability, enabled the authors to derive the relationship

$$S^*_{w,imb} = S^*_{w,dr} - \frac{1}{2} S^{*\,2}_{w,dr} \tag{1}$$

between normalized imbibition, $S^*_{w,imb}$, and drainage, $S^*_{w,dr}$, water saturations with equivalent oil relative permeability, k_{row}. The Narr and Henderson model normalized saturation with the removal of immobile water. With a maximum normalized water saturation of unity, the authors suggest that

$$S_{orw} = S_{oi} / 2 \tag{2}$$

as a limiting case. In reality, a threshold saturation must be achieved in the nonwetting phase to establish a connected pathway for nonwetting phase flow in a macroscopic sense. The use of Equation (2) as a rule-of-thumb, should be tempered with an understanding of the pore-level model for porous media and the flow function model assumed in its development.

Agarwal[2] addressed the relationship between initial and final gas saturations from an empirical perspective. He worked with a database of 320 imbibition experiments from published and unpublished sources. Agarwal further segmented the database to develop curve fits for common rock classifications: consolidated sandstones, limestones, unconsolidated sandstones, and sands. Although he eventually gave different empirical fits for unconsolidated sandstones and sands, he proposed the following simple relationship for the combined classes.

$$S_{gr} = 0.1813\, S_{gi} + 0.096071 \tag{3}$$

where S_{gr} is the residual gas saturation, and S_{gi} is the initial gas saturation. Note that the maximum implied residual saturation with Agarwal's equation was around 28%. Agarwal's database of supplementary information was limited to porosity and absolute permeability.

Land[3] noted that available data seemed to fit very well to an empirical functional form given as

$$S_{gr}^{*} = \frac{S_{gi}^{*}}{1+\left(\frac{1}{S_{gr}^{*\max}}-1\right)S_{gi}^{*}} \tag{4}$$

Land also used saturations normalized to discount immobile water. His equation refers to gas trapping, but he claimed the equivalent expression also applies to oil. Note the only free parameter is the maximum observable trapped nonwetting phase saturation corresponding to S_{gr}^{*} (S_{gi}^{*} = 1). This expression does not predict residual phase saturation -- only how residual saturation scales with initial saturation. The Land expression is assuredly the most commonly used expression of its type in reservoir engineering calculations.

DEVELOPMENT

Network Modeling

A pore-level network model capable of capillarity-based drainage and imbibition simulations was developed[4] which could make direct use of 3-D digital images of reservoir rocks from computed microtomography, CMT, as input. Within the constraint of image resolution (1.3 μm) and network model assumptions, nonwetting phase trapping during simulated imbibition could be followed on an incremental basis at the pore level. With such a powerful tool, studies of the relationship between initial and final nonwetting phase saturations could easily be performed, provided a database of pore structures could be obtained.

Realistic pore-level renderings of porous media can be generated which honor certain statistics gathered from real rock data[5-8]; however, this work utilized a small database of high permeability (> 500 md) sandstone CMT images gathered on appropriate facies types for such studies[9]. An example is furnished in Figure 1a. Our investigation was centered upon mostly clean, unconsolidated, water-wet sandstone from a fluvial deltaic environment. CMT data, for the most part, consisted of 3-D images, typically at 10 μm resolution, of 2-3 mm microcores bored from parent material which had been epoxy impregnated under confining stress. A suite of channel sand CMT images were examined, along with a Berea sandstone and a relatively clean Brent sample. Images were manually thresholded into binary images of rock versus pore space at the spatial resolution at which the CMT data was acquired, with sample porosity as a guiding factor. The resolution of acquired images was prescribed with a rule-of-thumb to place 3-5 voxels within the smaller intergranular pore throats. Microporosity was not detectable at this resolution, but the particular application was for relatively clean, quartz-grained, reservoir rocks. Digital sample sizes varied from 73*x*128*x*128 voxels to 180*x*217*x*217 voxels, with even larger volumes possible, as data acquisition and handling issues were resolved. Binary data CMT sets were passed to network model for direct computations at the image resolution.

Readers are refered elsewhere[4] for details concerning the network model, but a brief synopsis is supplied. Initial saturations were established via primary drainage simulation. In the network model, the nonwetting phase saturation is established as the union of all spheres with a curvature defined by the capillary pressure which had at least one connected pathway to predefined mass transfer surfaces. These surfaces could be defined as the external boundaries of the CMT volume or any internal plane. Regardless, these surfaces were the entrance and exit points for material transfer into or out of the pore network. An entire drainage capillary pressure curve could be constructed with the specification of a suite of sphere radii with steps in P_c ultimately determined

by the resolution of the CMT data set. An example of a network model-derived fluid distribution resulting from primary drainage simulation is shown in Figure 1b, where white indicates the low initial water saturation distribution.

Network model imbibition simulation in a assemblage of arbitrarily-shaped porosity elements was more complex. The roughness of pore wall elements precluded the ability to locally define a second radius of curvature to capture convex, wetting "film" shapes. Rather, imbibition simulation retraces the steps of drainage with an additional check for loss of nonwetting phase connectivity. It is the sudden loss of connectivity during a decrease in capillary pressure that traps pore-size segments of nonwetting phase. The network model will not allow movement of fluid with no connection to a defined mass transfer surface. No actual dynamics were included, only the progression from one capillary equilibrium condition to another. An example of a network model-derived fluid distribution resulting from primary imbibition simulation is shown in Figure 1c, where the residual oil is shown in black.

Kinetic phenomena associated with snap-off[10] are excluded from the model, but it can be noted that liquid bridges formed because of local variation in curvature are inherently unstable under the conditions prevailing during which they are formed in drainage[11,12]. While kinetics may be essential to model foam behavior in porous media, they were neglected here due to the absence of added surface active stabilizing agents. The phenomena of phase trapping during imbibition does constitute an interfacial instability event with an inherent "snapping off" of the nonwetting phase at pore throats. This process is presumed to be an instantaneous one upon capillary pressure reduction requiring no induction period under which pore contents could partially "leak out".

With the described drainage and imbibition sequences, sensitivities of the final state of imbibition (P_c=0) could easily be tested with respect to the maximum capillary pressure applied during primary drainage. Although entire capillary pressure curves were attained, the focus of this investigation concerned only the endpoints. However, with the interest in sensitivity to initial saturation, the study had an underlying goal of quantifying incremental trapping. Alternatively stated, what is the fate of each unit of saturation added to the nonwetting phase? For each bit of nonwetting phase composing the initial "oil" saturation, a portion will become trapped. Incremental trapping potential, dS_{or}/dS_o, is expected to be a function of saturation. Network modeling gave access to these quantities for comparison with the implied relationships from other $S_{or}(S_{oi})$ models.

The database of CMT samples included 7 samples: 5 unconsolidated sandstones representing channel facies types, 1 Berea sandstone, and 1 North Sea Triassic consolidated sandstone. Properties for each sample are furnished in Table 1. Typically, for each sample, four network model simulations were performed to relate S_{or} and S_{iw}, corresponding to four different designations of the mass transfer surface. These entrance/exit planes were placed at 0, 25, 50, and 75% through the CMT volume to reduce bias introduced by finite size effects.

Laboratory Measurements

A number of experiments on reservoir cores were initiated concurrently to test model predictions. These unconsolidated to weakly consolidated sandstone samples represented a broad range of facies types in a deltaic environment. A list of sample properties is provided in Table 2. Core plugs were cut with liquid nitrogen as the carrier fluid from frozen core and kept under confining stress of 1500 psi. Core plugs were subjected to standard solvent cleaning procedures. In displacement experiments, mineral oil was substituted for crude oil since water-wet conditions prevailed. Cleaned core plugs, typically 3 inches long and 1.5 inches in diameter, were subjected to waterflood displacement tests with two separate procedures to set the initial water saturation.

The first involves reduction of water saturation through displacement by oil in an overburden pressure cell. Oil was injected until water production ceased. The oilflooding method for core preparation does not usually yield low water saturations, as momentum applied to the oil phase is not necessarily efficiently transferred to the water phase to drive it out. Alternatively, the samples were prepared to a low initial water saturation condition via porous plate desaturation. A common value of capillary pressure (20 psi) was used to prepare all porous plate samples for waterflooding. Two samples were waterflooded a second time following porous plate desaturation as an internal quality control check.

It should be noted that the network model applies strictly to capillary-controlled $S_{orw}(S_{iw})$ predictions. Dynamic capillary pressure is not a well understood phenomena, but a network model built to explore sensitivity with respect to different static capillary pressure initial conditions is being used to compare results using one static and a second dynamically set S_{iw}.

RESULTS

Network Model Predictions

Results from the network model calculations are shown in Figure 2 and show a significant range in trapped nonwetting phase saturation. Different samples indicated similar trends but with different plateau values. The data were collapsed by normalizing residual oil saturations with respect to the maximum or plateau value.

A correlation was developed based upon the composite results.

$$S_{or}^{*} = erfc\left[1.4\left(erf^{-1}(S_{iw}^{*}) - 0.251\right)\right] \qquad (5)$$

This correlation is plotted in Figure 3 along with all scaled network modeling predictions, indicating an S-shaped relationship between starting and final conditions. Excellent consistency is observed for all samples, including the 2 consolidated sandstones.

Coreflood Studies

Considerable scatter was observed in experimental observations, in many cases outside of the limits of demonstrated reproducibility. Repeated measurements on two samples showed that residual oil saturation could be reproduced within 3-4 saturation units. The data are summarized in Table 2.

MODEL COMPARISONS

The empirical model developed from pore-level network model simulations was compared to the three previously described models from the literature. Figure 4 shows a comparison of the four models predicting normalized residual oil saturation given initial water saturation. For the Land model[3], a realistic choice of 35% residual was chosen as the maximum observable value in order to make this comparison. Note the Land[3] and Narr and Henderson[1] models are quite close to one another in their predictions, even though the Narr and Henderson model is not really applicable for the lower initial water saturations. It is unlikely that the oil relative permeability would be zero under primary drainage at such high oil saturation. The Agarwal model[2] is linear and does not share the common point of zero oil trapping at zero initial oil saturation. The network model-based correlation is the only one indicating a change in the sign of curvature. This occurs at roughly 60% initial water saturation.

On a more interesting note, the incremental trapping potential, dS_{or}/dS_{o}, is plotted in a normalized fashion in Figure 5. Here we see how trapping changes with overall saturation. The

Agarwal correlation predicts a constant trapping potential over the whole range of saturation. That is, all contributions to the initial oil saturation are equally likely to be trapped, whether they are added at low or high overall initial oil saturation. The Narr and Henderson model predicts a linear increase in incremental trapping potential with initial water saturation. The Land model has the same trend, but with a pronounced curvature. Both models predict that trapping is much more likely for initial amounts of nonwetting phase introduced. At high initial oil saturations, each added saturation unit carries a lower probability of being trapped during subsequent imbibition. Notably, the Narr and Henderson model passes through the origin, while the Land model predicts a sensitivity in incremental trapping potential even in the limit of S_{oi}^{*} 100%. The network model-based correlation is the only model indicating a local maximum.

We observe the following main points with regard to the newly proposed correlation:

- Incremental trapping potential varies with saturation.
- Residual nonwetting phase saturation is most sensitive to mid-range initial saturations.
- Trapping becomes a weak function of initial saturation at both small and large S_{iw}.

It is acknowledged that predictions at very high initial water saturation values are probably not of economic interest to the industry. It is also questionable that predictions for S_{orw} with S_{oi} below the percolation limit are of practical interest. The model does, however, predict that efficiency of withdrawal of nonwetting phase prior to reaching the percolation threshold decreases as more nonwetting phase is placed into the pore system, with the first "drop" of oil being completely retractable.

COMPARISON WITH EXPERIMENTS

The network model results were used to guide the process of rescaling experiments performed at one initial water saturation to another for the same core sample. The model was used to predict the maximum observable residual oil saturation given coreflood results with higher initial water saturation. The model was also used in a forward sense to predict the lowering of residual oil saturation by having more water initially present given displacement results at immobile water saturation. The measured and predicted values for the two cases are plotted in Figure 6. For these calculations, it was assumed that the porous plate sample preparation procedure yielded the immobile water saturation and the subsequent waterflood gave the maximum residual oil saturation. Figure 6 shows remarkable agreement, in light of experimental reproducibility and the use of dynamic displacement to establish the higher initial water saturation conditions. Additional experimental data beyond the two point tests would have been helpful in the comparison. Still, the proposed model is consistent with available observations and provides an avenue to rescale data for conditions other than those represented in a single test.

DISCUSSION

The observed trends are explained within the context of reversible and irreversible motions of the fluid-fluid interface. During imbibition, only disconnection at pore throats is seen to reduce nonwetting phase connectivity. Other fluid movement events are seen to be a result of "elastic' rebounding of fluid-fluid interfaces. As long as connectivity to a mass transfer surface is maintained, the nonwetting phase is allowed to conform to its preferred shape and orientation, with excess fluid draining into the "outlet". With no internal resistance for water migration, this process is modeled as an instantaneous one. Nonwetting phase trapping occurs whenever the final conduit for nonwetting phase withdrawal is disconnected due to a change in governing curvature imposed by the prevailing capillary pressure.

The concept of reversible and irreversible interface motion is most easily illustrated with idealized topologies, each representing different elemental contributions to a capillary pressure curve. In Figure 7a, we see a wedge-shaped porosity element which might be ascribed to grain contacts, corners, or roughness. If we envision a process of capillary pressure elevation and relaxation, aside from possible stick-slip phenomena[13,14] at the three phase contact line, pore-filling and emptying produces no interfacial instability. We refer to this conforming/rebounding fluid-fluid interface motion as reversible – in a mechanical and not a thermodynamic sense. This type of fluid interface motion contributes to the capillary pressure-saturation relationship. For intergranular porosity systems, it can account for a significant portion of the saturation change with capillary pressure at high capillary pressure. Contact angle hysteresis may well be present such that interface position may be a more complex function of applied capillary pressure, but no trapping is seen.

However, in Figure 7b, we see nonwetting phase stranding in a multi-pore topology following a simple pore-level drainage and imbibition cycle. Within the context of the pore network, it is actually this kind of irreversible event which is used to identify individual pores. Contact angle hysteresis may also be a factor in this process, but the only interesting new phenomena which may be introduced occurs in those systems which have advancing and receding angles on opposite sides of 90º.

Thus, for water-wet rocks containing almost exclusively intergranular porosity, we propose a pore-level interpretation of a typical capillary pressure curve consistent with network modeling observations. In Figure 8, the saturation is loosely broken into three dominant regimes. The lower saturation range is primarily where a percolating network of nonwetting phase is formed during primary drainage. The first addition of nonwetting phase is "perfectly" reversible, with more phase trapping possible upon imbibition as more nonwetting phase is introduced. This first saturation range may be unattainable upon imbibition for water-wet rocks due to connectivity considerations. In the middle range of saturation, the largest number of true multipore events take place, each with the potential of stranding nonwetting phase upon imbibition. At the higher capillary pressure levels, fluid uptake still involves intrusion into some new small pores, but it also is characterized by fluid-fluid interfaces conforming to surface roughness in previously invaded pores. This latter fraction produces no nonwetting phase trapping upon imbibition. The location of the boundaries in Figure 8 are for illustration purposes only, as a gradual transition is expected from one type of dominant contribution to another. This interpretation has significant implications for those using the primary drainage curve to infer "pore or throat size distributions."

Rocks with multimodal porosity, e.g. microporosity, will contain porosity features which have nonwetting phase trapping potential into the high capillary pressure range. Multi-step relationships might then be expected in the relationship between residual nonwetting phase and initial saturation conditions. Phase trapping, however, would be a function of spatial arrangement and not simply pore type.

In a similar light, these results are restricted to nonwetting fluids with no inherent wettability alteration potential. It has been suggested that the stability of intervening water films is important in preventing wettability alteration[15-17]. Should pore surfaces become chemically altered such that the roles of wetting and nonwetting phase are interchanged locally, the results of this paper do not apply. The same network model employed here has been shown to work for such mixed wettability cases using the concept of two interacting networks[4]: one water-wet and the other oil-wet. This type of study is beyond the scope of this investigation; however, the network model assumption of no impaired mobility of the wetting phase suggests no permanent trapping of oil in the oil-wet network. More rigorous computational methods[18,19] are available for extremely complex inputs beyond the reach of simple rule-based networks.

CONCLUSIONS

Clean, water-wet sandstones consisting predominantly of intergrannular porosity were observed to show little sensitivity to initial water saturation in the low initial water saturation region in experiments and network model computations utilizing 3-D, pore-level renderings of real rock pore space. A new S-shaped correlation was constructed based upon network modeling results which indicated most pore trapping of nonwetting phase occurs in the mid-saturation range upon imbibition in reservoir rocks of this type. The new correlation is significantly different than literature correlations proposed by Narr and Henderson[1], Agarwal[2], and Land[3] which also, to a large degree, were developed for similar rock types.

Interpretation of trapping and nontrapping elemental contributions to the capillary pressure-saturation relationship has significant implications for those using primary drainage capillary pressure data to infer pore or throat size distributions. Filling of porosity elements by nonwetting phase at high capillary pressure were interpreted as surface roughness filling events with no nonwetting phase trapping potential upon imbibition for clean, water-wet, intergranular porosity sandstone.

The new correlation can be used to scale limited experimental data to other conditions or correct data acquired at inappropriate conditions. Reliable estimates of trapped nonwetting phase saturation can be supplied by the newly developed correlation for clean, water-wet, intergranular porosity sandstones for both reserve calculations and normalization of flow functions within the context of reservoir simulation. Extrapolation of the prescribed correlation to describe displacement efficiency in multimodal porosity rocks or oil-wet conditions is not recommended.

NOTATION

DCB	distributary channel bar facies type
k	medium permeability
k_{row}	oil relative permeability in a water-oil displacement
P_c	capillary pressure
S_{gi}	initial gas saturation
S_{gr}	residual gas saturation
S_{iw}	initial water saturation
S_j^*	saturation of phase j normalized to remove immobile water
S_{oi}	initial oil saturation
S_{orw}	residual oil saturation to waterflooding
S_{orw}^{max}	maximum observable residual oil saturation to waterflooding
S_{wi}	immobile water saturation
$S^*_{w,imb}$	normalized water saturation under imbibition with oil relative permeability, k_{row}
$S^*_{w,dr}$	normalized water saturation under drainage with oil relative permeability, k_{row}
TCB	tidal channel bar facies type
ϕ	medium porosity

ACKNOWLEDGEMENTS

Authors wish to gratefully thank R. Al-Hussainy and K. Sampath for their suggestions and support. We thank Mobil Technology Company and Mobil E&P Technical Center management for granting permission to publish.

REFERENCES

1. Naar, J. and Henderson, J. H., "An Imbibition Model – Its Application to Flow Behavior and the Prediction of Oil Recovery," *Society of Petroleum Engineers Journal*, (1961) June, 61-70.
2. Agarwal, R. G., *Unsteady-State Performance of Water-Drive Gas Reservoirs*, Ph.D. Dissertation, Texas A&M University, 1967, 46-59.
3. Land, C. S., "Calculation of Imbibition Relative Permeability for Two- and Three-Phase Flow From Rock Properties," *Society of Petroleum Engineers Journal*, (1969) June, 149-156.
4. Hazlett, R. D., "Simulation of Capillary-Dominated Displacements in Microtomographic Images of Reservoir Rocks," *Transport in Porous Media*, (1995) **20**(1/2), 21-35.
5. Adler, P. M., Jacquin, C. G., and Quiblier, J. A., "Flow in simulated porous media," *International Journal of Multiphase Flow*, (1990) **16**, 691-712.
6. Ioannidis, M., Kwiecien, M., and Chatzis, I., "Computer generation and application of 3-D model porous media: from pore-level geostatistics to the estimation of formation factor," SPE paper 30201 presented at the Society of Petroleum Engineers Petroleum Computer Conference, Houston, 1995, 185-194.
7. Bakke, S. and Øren, P. E., "3-D Pore-Scale Modelling of Heterogeneous Sandstone Reservoir Rocks and Quantitative Analysis of the Architecture, Geometry and Spatial Continuity of the Pore Network," SPE paper 35479 presented at the European 3-D Reservoir Modelling Conference, Stavanger, April 16-17, 1996.
8. Hazlett, R. D., "Statistical Characterization and Stochastic Modeling of Pore Networks in Relation to Fluid Flow," *Mathematical Geology*, (1997) **29**(6), 801-822.
9. Coles, M. E., Hazlett, R. D., Muegge, E. L., Jones, K. W., Andrews, B., Dowd, B., Siddons, P., Peskin, A., Spanne, P., and Soll, W. E., "Developments in Synchrotron X-Ray Microtomography With Applications to Flow in Porous Media," *SPE Reservoir Evaluation & Engineering*, (1998) August, 288-296.
10. Roof, J. G., "Snap-Off of Oil Droplets in Water-Wet Pores," *Society of Petroleum Engineers Journal*, (1970) March, 85-90.
11. Falls, A. H., Gauglitz, P. A., Hirasaki, G. T., Miller, D. D., Patzek, T. W., and Ratulowski, J., "Development of a Mechanistic Foam Simulator: The Population Balance Approach and a Description of Generation by Capillary Snap-Off," SPE paper 14961 presented at the SPE/DOE Enhanced Oil Recovery Symposium, Tulsa, April 20-23, 1986.
12. Sanchez, J. M. and Hazlett, R. D., "Foam Flow Through an Oil-Wet Porous Medium: A Laboratory Study," SPE paper 19687 presented at the 64th Annual Technical Conference and Exhibition of the Society of Petroleum Engineers, San Antonio, October 8-11, 1989, 579-588.
13. Dussan V., E. B. and Davis, S. H., "On the motion of a fluid-fluid interface along a solid surface," *Journal of Fluid Mechanics*, (1974) **65**, part 1, 71-95.
14. Hazlett, R. D., "On surface roughness effects in wetting phenomena," *Journal of Adhesion Science and Technology*, (1992) **6**(6), 625-633.
15. Melrose, J. C., "Interpretation of Mixed Wettability States in Reservoir Rocks," SPE paper 10971 presented at the 57th Annual Technical Conference and Exhibition of the Society of Petroleum Engineers of AIME, New Orleans, September 26-29, 1982.
16. Hirasaki, G. J., "Wettability: Fundamentals and Surface Forces," SPE/DOE paper 17367 presented at the SPE/DOE Enhanced Oil Recovery Symposium, Tulsa, April 17-20, 1988.
17. Ward, A. D., Ottewill, R. H., and Hazlett, R. D., "An Investigation into the Development of Mixed Wettability States," Proceedings of the 5th International Symposium on the Evaluation

of Reservoir Wettability and Its Effect on Oil Recovery, Trondheim, June 22-24, 1998, 320-328.
18. Hazlett, R. D., Chen, S. Y., and Soll, W. E., "Wettability and rate effects on immiscible displacement: Lattice Boltzmann simulation in microtomographic images of reservoir rocks," *Journal of Petroleum Science and Engineering*, (1998) **20**, 801-822.
19. Ferréol, B. and Rothman, D. H., "Lattice-Boltzmann simulations of flow through Fontainebleau Sandstone," *Transport in Porous Media*, (1995) **20**(1/2), 3-20.

Table 1. Description of porous media in the CMT database.

Sample ID	**Core Plug Permeability, md**	**CMT Image Porosity, ϕ**	**CMT Image Resolution, μm**	**CMT Dimensions, voxels**
Berea	1100	0.178	10	128 *x* 128 *x* 128
TCB 1	6000	0.320	10	95 *x* 128 *x* 128
DCB 1	7400	0.179	20	108 *x* 145 *x* 145
TCB 2	5800	0.248	15	234 *x* 146 *x* 146
DCB 2	20,000	0.247	30	73 *x* 128 *x* 128
TCB 3	2000	0.179	10	95 *x* 128 *x* 128
North Sea Triassic	470	0.160	2.7	180 *x* 217 *x* 217

Table 2. Core plug samples and experimental program results.

Sample ID	**Facies Type**	**Porosity ϕ**	**Permeability md**	*S_{iw} Set Via Oilflood*		*S_{iw} Set Via Porous Plate*	
				S_{iw}	**S_{orw}**	**S_{iw}**	**S_{orw}**
1	distributary channel bar	0.319	12,500	0.070	0.168	0.045	0.212
2	distributary channel bar	0.277	6400	0.359	0.324	0.184	0.332
3	lower delta plane channel/mouthbar	0.285	4700	0.232	0.332	0.083	0.346
4A	shoreface	0.327	3200	0.311	0.228	0.102	0.258
4B	shoreface	0.327	3200	0.311	0.228	0.092	0.288
5	shoreface	0.314	3900	0.270	0.339	0.078	0.325
6	shoreface	0.357	5900	0.333	0.282	0.073	0.442
7	lower shoreface	0.341	4600	0.392	0.254	0.143	0.356
8A	lower shoreface	0.288	1000	0.389	0.172	0.150	0.279
8B	lower shoreface	0.288	1000	0.389	0.172	0.168	0.238
9	lower shoreface	0.298	750	0.179	0.189	0.136	0.182
10	lower shoreface	0.308	760	0.269	0.210	0.107	0.152

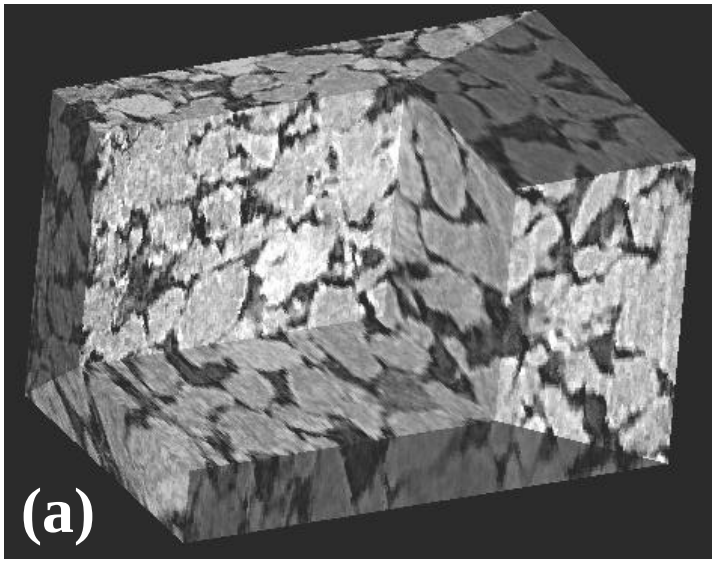

Figure 1. Example CMT volume and network model results: (a). Rectangular CMT volume with excavated section to reveal inner detail. Note pore space is dark and grains are grey, (b). The same CMT volume processed to display a low water saturation distribution (white) in the pore space as a result of network model primary drainage simulation, and (c). The same CMT volume indicating the distribution of residual nonwetting phase (black) following network model imbibition simulation.

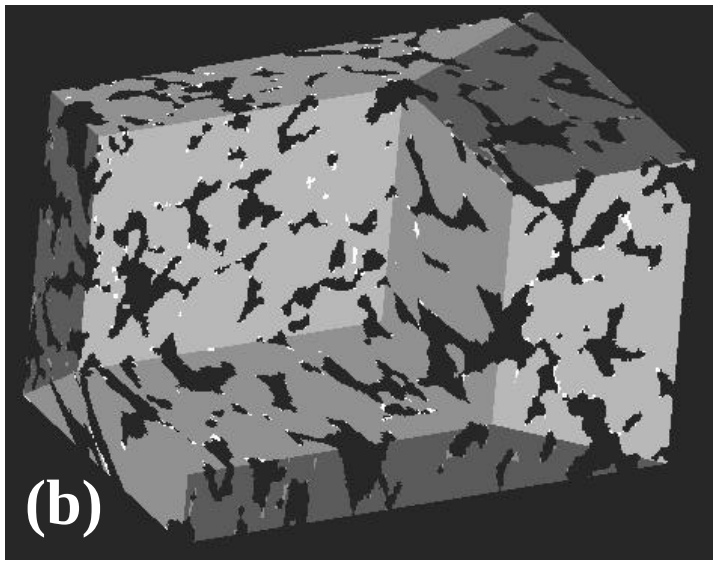

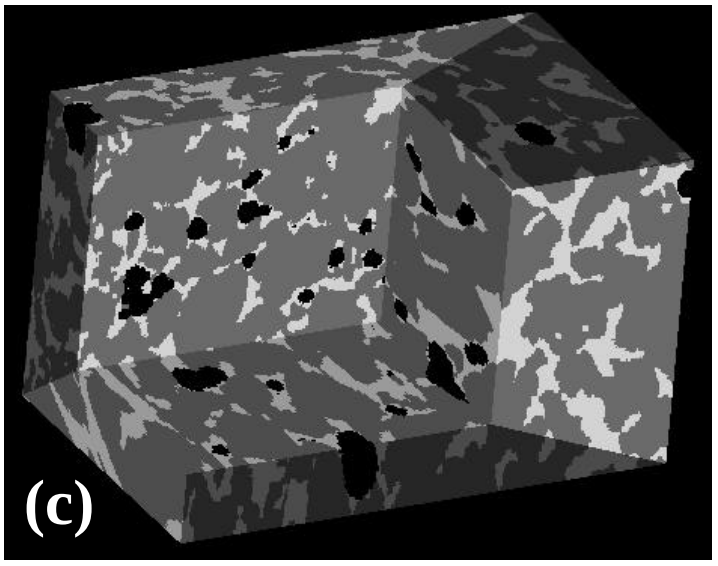

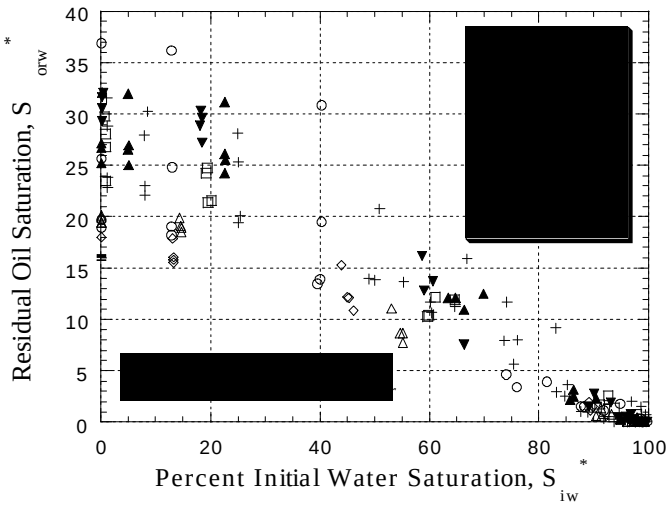

Figure 2. Network model predicted imbibition endpoints, indicating a band of possible endpoint saturations. Results are shown for 4 different mass transfer surfaces per CMT sample.

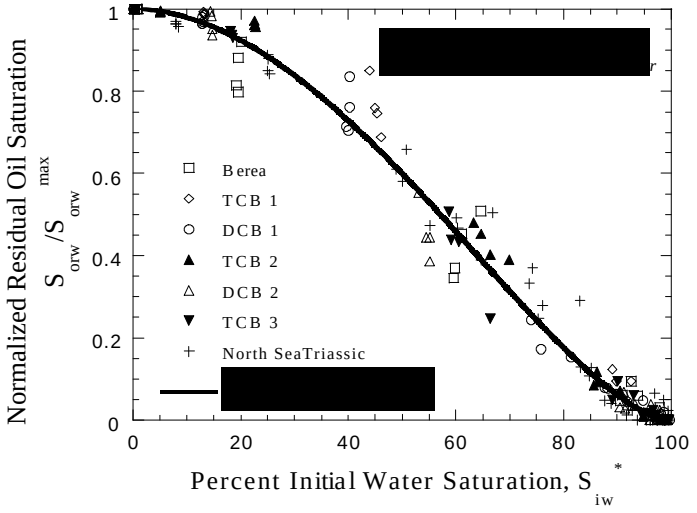

Figure 3. Network model predictions of normalized residual nonwetting phase saturation as a function of initial water saturation. The line represents an empirical fit to the data. Nonwetting phase saturation is normalized with respect to the maximum residual.

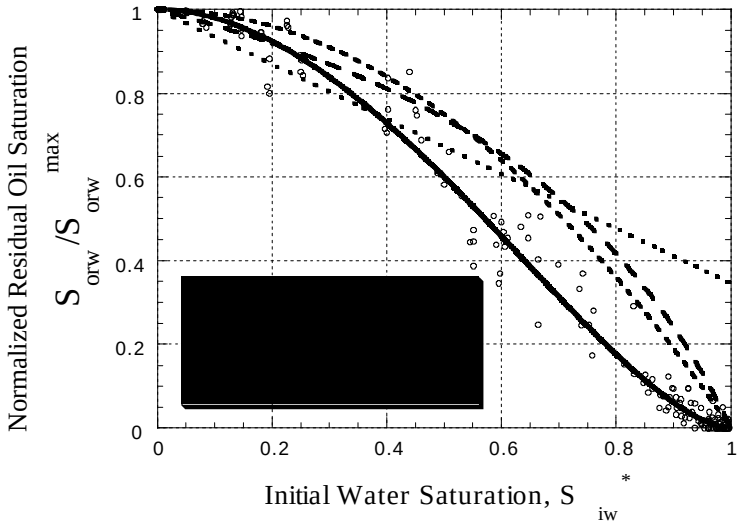

Figure 4. Comparison of the network model-based correlation with literature correlations for residual nonwetting phase saturation as a function of initial conditions.

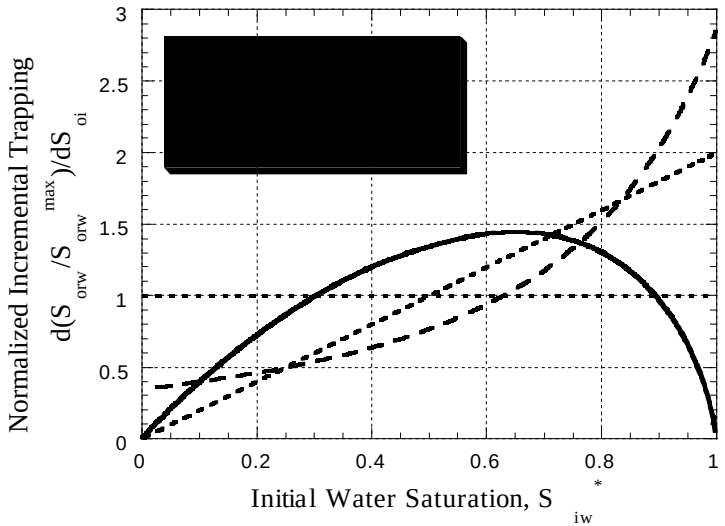

Figure 5. Comparison of the network model-based prediction of incremental trapping potential with literature correlations as a function of initial conditions.

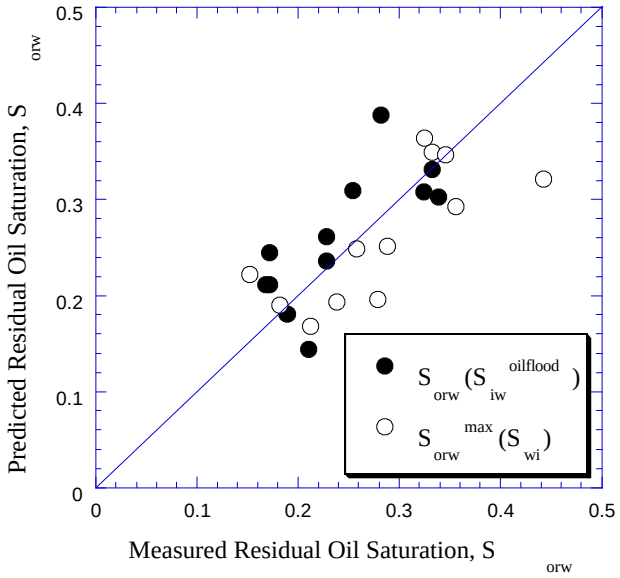

Figure 6. Waterflood residual oil saturations, S_{orw}, predicted from the network model-based correlation. Predictions are shown of the maximum residual oil saturation given test data from the waterflood where the initial saturation was prepared via an oilflood. Alternatively, predictions of $S_{orw}(S_{iw}^{oilflood})$ are also furnished given test data from the coreflood where the initial water saturation was established by the porous plate method. The model was used for normalized saturations with the assumption that the porous plate-established water saturation represented the immobile water saturation ($S_{iw}^{porous\ plate} = S_{wi}$).

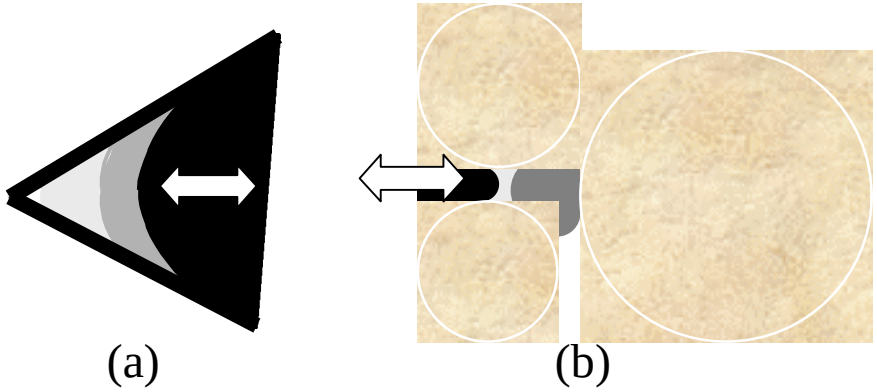

Figure 7. Model porosity types which contribute to the capillary pressure-saturation relationship: (a) roughness with no trapping potential [reversible] and (b) multipore elements with significant trapping potential [irreversible].

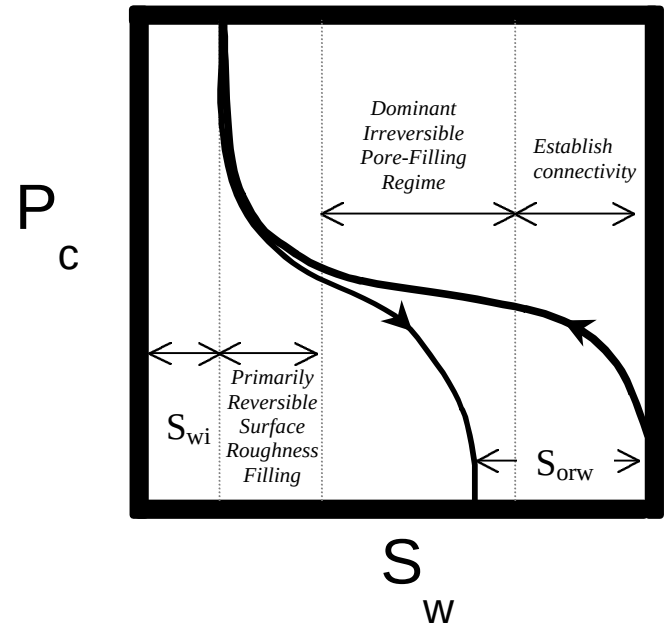

Figure 8. An illustrative capillary pressure curve with designated dominant trapping/nontrapping regimes for clean, water-wet intergranular porosity sands / sandstone